EPJ Web of Conferences **293**, 00028 (2024) https://doi.org/10.1051/epjconf/202429300028
*mm Universe 2023*

# Projection effects on pressure profiles: A case study of the Virgo replica

T. Lebeau[1,*], J.G. Sorce[2,1,3], and N. Aghanim[1]

[1]Université Paris-Saclay, CNRS, Institut d'Astrophysique Spatiale, 91405 Orsay, France
[2]Université de Lille, CNRS, Centrale Lille, UMR 9189 CRIStAL, 59000 Lille, France
[3]Leibniz-Institut für Astrophysik (AIP), An der Sternwarte 16, 14482 Potsdam, Germany

**Abstract.** An accurate mass calibration of galaxy clusters is a crucial step towards precise constraints on the cosmological parameters $\sigma_8$ and $\Omega_m$ from clusters. Cluster masses can be estimated assuming hydrostatic equilibrium, but several physical and observational effects can alter this calculation. One of those are projection effects which are the focus of our present analysis. We present a case study of the simulated Virgo cluster, extracted from the CLONE constrained simulation. We study Virgo pressure and electron density quantities projected along different directions, including along the Milky Way-Virgo axis which mimics our observation direction. We show two main projection effects: the role of the integrated mass along the line of sight (LoS) in each chosen direction, including the presence of massive objects, and the signature of small scale physics in the core of the cluster along these directions.

## 1 Introduction

Galaxy clusters are formed via the gravitational collapse of primordial over-densities and they are therefore peaks of density in the matter distribution of the Universe. Their number count is thus a probe for the cosmological parameters provided their masses are accurately estimated. Any massive cluster contains a hot Intra-Cluster Medium (ICM) emitting in X-rays via bremsstrahlung [1, 2]. The ICM can also be observed in the sub-millimeter domain through the thermal Sunyaev-Zel'dovich (tSZ) effect [3]. Assuming the hydrostatic equilibrium between the ICM pressure and the gravitational potential well, we can estimate the hydrostatic mass of a galaxy cluster [4].

The hydrostatic equilibrium hypothesis is most often invalid and leads to a so-called hydrostatic mass bias. There are multiple possible contributions to the hydrostatic mass bias (e.g. non-thermal pressure, asphericity, unrelaxedness,...) that needs to be well calibrated in order to reach an accurate mass estimation. In fact, the value of the bias is still debated. On the one hand, there is a large scatter around $(1 - b) = 0.8$ among the values proposed by several cosmological simulations or weak lensing experiments as shown in [5]. On the other hand, the value proposed by [5] to reconcile the CMB and tSZ number counts constraints on the parameters $\sigma_8$ and $\Omega_m$ is $(1 - b) = 0.62 \pm 0.07$. In addition to physical sources of biases, we can have an observational bias. Since we can only observe the ICM of clusters from our

*e-mail: theo.lebeau@universite-paris-saclay.fr

unique position in the Universe, reconstructed thermodynamical properties of clusters can then be affected by the presence of gas along the LoS. This work focuses on those projection effects. Using constrained cosmological simulations, we can quantify the projection effects by observing galaxy clusters from multiple positions. To this aim, we use a hydrodynamical simulation replica of the Virgo cluster [6]. Quantifying the projection effects on this object is a first step towards a better understanding of the sources of biases on the cluster population.

In section 2, we briefly introduce the Virgo replica as well as the pressure maps. We present 2D radial profiles extracted from projected pressure maps and the 3D-deprojected radial profiles derived using a geometrical deprojection method in section 3. We discuss the projection effects in section 4. This proceeding summarizes only briefly the method. Instead, it focuses on the results. Details can be found in [7]. Moreover, we only present pressure radial profiles, electron density profiles can also be retrieved in [7].

## 2 Virgo replica

We start with a short presentation of the CLONE (Constrained LOcal and Nesting Environment) simulation used in this work. This high-resolution zoom-in hydrodynamical simulation of Virgo was produced using the adaptive mesh refinement code *RAMSES*[9]. The evolving initial conditions of this simulation are that of the Local Universe, they were constrained with both observed galaxy positions and peculiar velocities,[8]. For this run, the *Planck* cosmology from [10] was adopted with spectral index $n_s = 0.961$, total matter density $\Omega_m = 0.307$, dark energy density $\Omega_\Lambda = 0.693$, baryonic density $\Omega_b = 0.048$, Hubble constant $H_0 = 67.77$ km/s/Mpc, and amplitude of the matter power spectrum at 8 Mpc/h, $\sigma_8 = 0.829$. The zoom region, contained in the 500 Mpc/h Local Universe box [8], is a 30 Mpc diameter sphere with a resolution of $8192^3$ effective dark matter (DM) particles of mass $m_{\rm DM} = 3.10^7$ $M_\odot$. On the baryons side, the finest cell size is 0.35 kpc. The sub-grid physical models for radiative gas cooling and heating, star formation, kinetic feedback from type II supernovae and Active Galactic Nuclei (AGN) follow the Horizon-AGN implementation of [11, 12]. In addition, the AGN-jet is oriented according to the black hole spin [see 13, for details]. Our study focuses on the ICM gas, we thus select the cells with a temperature above $10^5$ K and remove the cells associated to the galaxies. More precisely, we delete the cells within the virial radius of the DM halo associated to the galaxies, with a mass above the completeness threshold of the simulation. We only keep the central galaxy of the cluster, M87, its DM halo being the cluster halo.

Four directions are considered in our study, they are associated to projected maps: 1) along the LoS from the center of the large scale simulation box to the Virgo cluster (*Cen* hereafter). The large scale simulation is almost centered on the Milky way [8], we thus assume that this projection is comparable to the real observation of the Virgo cluster, as shown in [14]; 2) along the main filament connected to Virgo in order to study the impact of the gas distribution along the LoS on the reconstructed radial pressure profiles (*Fil* hereafter); 3) and 4) orthogonally to the main filament. These are two extreme cases with less mass along the LoS. They are both perpendicular to the main filament and respectively follow a rotation around the x (*Filx*) and y (*Fily*) axis.

The pressure maps are built using the mass weighted mean of the cells along the LoS in each pixel because pressure is an intensive quantity. In Fig. 1, we present the pressure maps along the four directions. These square maps are 22.123 Mpc wide centered on the center of mass of the cluster and contain $15728^2$ pixels of ∼1.4 kpc width. The inner (outer) circle

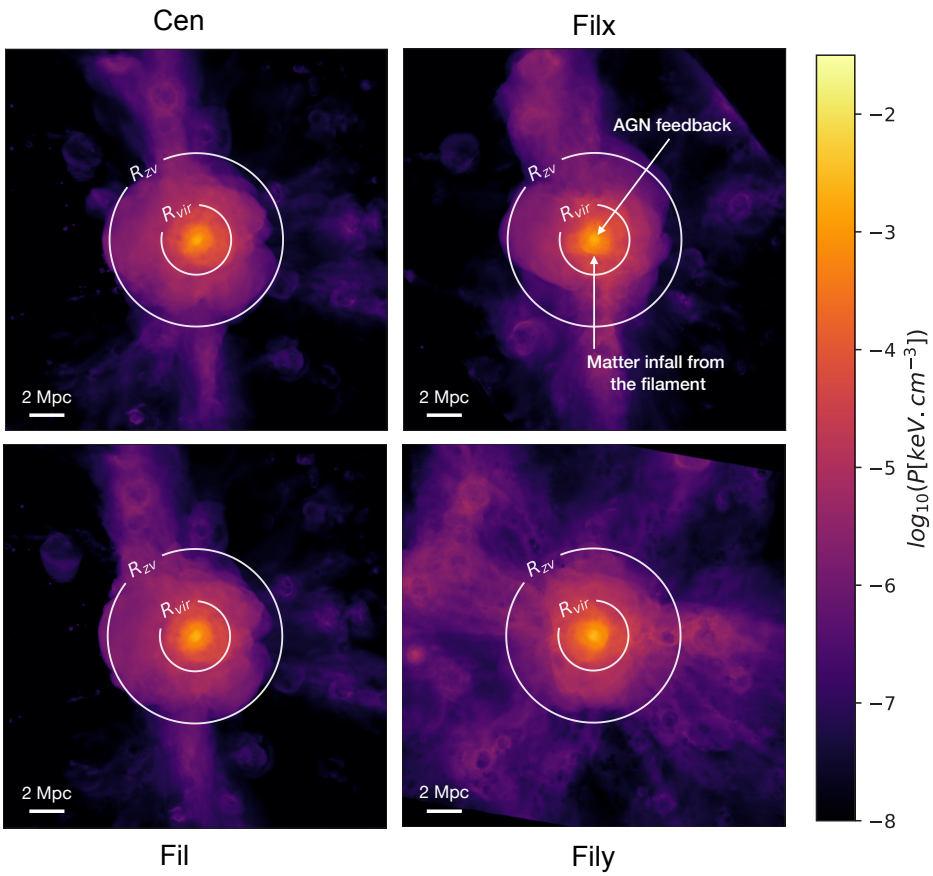


**Figure 1.** Pressure maps along four directions. The maps are 22.123 Mpc wide, they contain $15728^2$ pixels. The central circle is the virial radius, the outer one is the zero velocity radius. The color scale ranges from $10^{-8}$ to $10^{-1.5}$ kev.cm$^{-3}$. From top to bottom and left to right, the *Cen*, *Fil*, *Filx* and *Fily* projections. These maps show the matter distribution in Virgo's local environment. The cluster is part of a matter sheet (visible on the *Fily* projection) including a main filament (top of the *Filx* projection) and three secondary filaments (bottom of the *Filx* projection and top and bottom of the *Fil* and *Cen* projections). The white arrows in the top right panel show the pressure discontinuities due to the AGN feedback in the core and to the matter infall from the filament at ∼850 kpc from the core.

stands for the virial (zero velocity) radius (respectively $R_{vir}$ and $R_{zv}$, from [6]).

These maps show several features, both at large and small scales. At large scales, we observe the matter distribution in the Virgo environment. The *Fily* map highlights a large amount of high pressure (above $10^{-5}$ keV.cm$^{-3}$) beyond the zero velocity radius, whereas for the three other maps the high pressure is concentrated in filamentary structures. The *Fil* map exhibits a vertical filament that is thinner than the main one visible on the *Filx* map. It indicates that the matter is concentrated in a sheet crossing the cluster, this sheet is also visible on the *Fily* map. Moreover, the maps reveal differences in the cluster shape within the zero velocity radius, e.g. the *Filx*-map displays an elongated cluster, the spherical symmetry hypothesis is therefore strongly challenged in this case.

Within the virial radius of the *Filx*-map, there is a pressure discontinuity perpendicular to the main filament connected to the cluster (see the bottom white arrow in the top right panel of Fig.1). This is due to the accretion of the warm gas falling from the filament. This gas is heated while entering the cluster [see 15–17, and references therein for recent studies] and is then shocked [see 18, for a review on shocks in clusters]. In the center of the cluster, we observe another pressure discontinuity, more or less elliptical depending on the projection (see the top white arrow in the top right panel of Fig.1). This is due to the AGN feedback of the central galaxy of the cluster, M87. In this simulation, the AGN jet direction depends on the galaxy spin that is mainly perpendicular to the *Filx-direction*, the AGN feedback is thus oriented mainly along the *Filx*-direction. As a result, the pressure discontinuity is seen spherical in this projection (as we observe on the top-right panel of Fig. 1 ). On the contrary, in the other projections, we observe an elliptical pressure discontinuity. This pressure discontinuity has been observed in X-rays, the associated jet power has been estimated to be $F_{jet} \approx 3 \times 10^{42}$erg.s$^{-1}$ [19].

## 3 Radial profiles

In Fig.2 (left), we present the 2D radial profiles of pressure derived from projected maps. The profiles show the same trend from the outskirt to $R_{500}$: deviations arise in the central part of the cluster. In observations, we only have access to projected cluster quantities and we use deprojection techniques to retrieve 3D quantities. In this work, we adapt the non-parametric geometrical iterative deprojection method proposed by [20]. Figure 2 (right) shows the 3D-deprojected pressure profiles compared to the 3D radial profiles. The bottom panel shows the relative difference to the 3D profile. The pressure is very sensitive to projection effects, much more than the electron density as show in [**?** ]. Beyond 1 Mpc, the 3D-deprojected profiles are similar to the 3D profile and the deviations are within the error bars. Below $R_{500}$, we observe larger differences, up to more than 50%. We discuss the projection effects impacting both 2D and 3D-deprojected radial profiles below.

## 4 Projection effects

In this section, we discuss the impact of projection effects on the 2D radial profiles and 3D-deprojected radial profiles. We distinguish between two main effects: the role of the integrated mass along the LoS in each chosen direction, including the presence of massive objects, and the signature of small scale physics in the core of the cluster along these directions.

- Focusing on the 2D radial profiles in Fig. 2 (left), the *Fily*-projection has the highest pressure in the cluster core. On the contrary, the *Cen* projection exhibits the lowest pressure profile. We observe the same trend on 3D-deprojected profiles in the right panel in Fig.2 right. In fact, there are differences in the cumulative mass outside the cluster along each LoS [see Fig.8 of 7]. The *Fily* projection has the lowest amount of matter and pressure outside the cluster, that is outside $R_{vir}$ [see again Fig.8 of 7], whereas the *Cen* projection has the highest. The pressure in the pixels of the maps are mass-weighted means of the cells along the LoS. Consequently, if there is mass outside the cluster, the mean 2D radial pressure will be lower than the cluster single mean pressure because the pressure associated to this mass is orders of magnitude lower. This is coherent with what

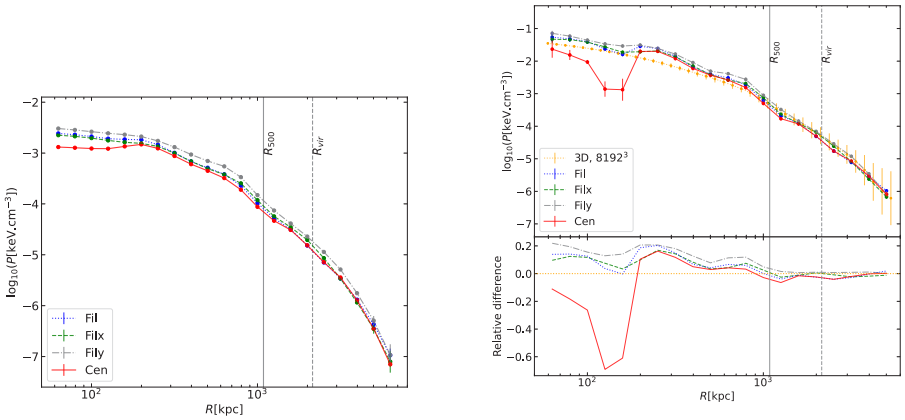


**Figure 2.** Left: 2D radial pressure profiles. Right: 3D radial pressure profiles in orange, compared to 3D-deprojected radial profiles. The bottom panel show the relative difference to the 3D profile. For both figures, the blue dotted profile is the *Fil* projection, the green dashed and grey dash-dotted profiles are the *Filx* and *Fily* projections respectively. The red solid profile is the *Cen* projection. The vertical solid line is $R_{500}$, the vertical dashed line is the virial radius.

we see in Fig. 2. To summarize, if there is more mass outside the cluster, the 2D and 3D-deprojected pressure profiles are lower.

- Moreover, we note an important decrease, nearly a reduction by a factor of two, on the pressure profile in the core of the cluster along the *Cen* projection 2D radial profile (Fig.2 left). This pressure decrease is even stronger on the 3D-deprojected profile (Fig. 2, right). Actually, a $\sim 10^{12}\mathrm{M}_{\odot}$ group of galaxies lies along this particular direction. This is most likely the simulated counterpart of the Canes Venaciti I group that is known to be close to the LoS between the Milky Way and the Virgo cluster [21–23].
- Pressure discontinuities are visible in the pressure maps. There are no discernible signatures of theses discontinuities in the 3D profiles. In the 2D pressure radial profiles displayed in Fig. 2 (left), we remark variations of the slope at around 250 and 850 kpc. We note an excess pressure at the same radii on the 3D-deprojected profiles (see Fig.2 right). The excess pressure at around 250 kpc is due to the AGN feedback ring visible on pressure maps. The second excess pressure, around 850 kpc, is due to the pressure discontinuity of the gas flowing from the filament into the cluster, as seen in the pressure maps. The deprojection process significantly enhances these pressure discontinuities.

## 5 Conclusion

This study of the Virgo cluster replica reveals the complex physics at play in its core and highlights different types of projection effects on its 2D and 3D-deprojected pressure profiles. We show that the pressure profiles are lower if there is more mass outside the cluster, particularly if a group of galaxies is in the LoS, and that pressure discontinuities are strongly emphasized by the deprojection process. It is a case study of a very specific unrelaxed cluster

considered as a first step of a larger project within the LOCALIZATION[1] collaboration. In this collaboration, we will study the contributions of different sources of biases on the mass determination for a large sample of galaxy clusters extracted from a constrained hydrodynamical cosmological simulation of the local Universe. We will then be able to compare the results to those of random simulations, and to actual observations.

## Acknowledgements

This work was supported by the grant agreements ANR-21-CE31-0019 / 490702358 from the French Agence Nationale de la Recherche / DFG for the LOCALIZATION project. The authors were also supported by funding of the ByoPiC project from the European Research Council (ERC) under the European Union's Horizon 2020 research and innovation program grant agreement ERC-2015-AdG 695561 (ByoPiC, https://byopic.eu). The authors thank the very useful comments and discussions with all the members of this project. They thank the Center for Advanced Studies (CAS) of LMU Munich for hosting the collaborators of the LOCALIZATION project for a week-long workshop. The authors gratefully acknowledge the Gauss Centre for Supercomputing e.V. (www.gauss-centre.eu) for providing computing time on the GCS Supercomputers SuperMUC at LRZ Munich. We finally thank Florent Renaud for sharing the *rdramses* RAMSES data reduction code.

## References

[1] C.L. Sarazin *et al.*, Reviews of Modern Physics **58** (1986), 1
[2] H. Böhringer *et al.*, arXiv preprint arXiv:0907.4277 (2009)
[3] R.A. Sunyaev *et al.*, Comments on Astrophysics and Space Physics **4** (1972), 173
[4] A.V. Kravtsov *et al.*, Annual Review of Astronomy and Astrophysics **50** (2012), 353
[5] L. Salvati *et al.*, Astronomy & Astrophysics **614** (2018), A13
[6] J.G. Sorce *et al.*, Monthly Notices of the Royal Astronomical Society **504** (2021), 2998
[7] T. Lebeau *et al.*, arXiv preprint arXiv:2310.02326 (2023)
[8] J.G. Sorce *et al.*, Monthly Notices of the Royal Astronomical Society **455** (2016), 2078
[9] R. Teyssier *et al.*, Astronomy & Astrophysics **385** (2002), 337
[10] Planck Collaboration, Astronomy & Astrophysics **571** (2014), A16
[11] Y. Dubois *et al.*, Monthly Notices of the Royal Astronomical Society **444** (2014), 1453
[12] Y. Dubois *et al.*, Monthly Notices of the Royal Astronomical Society **463** (2016), 3948
[13] Y. Dubois *et al.*, Astronomy & Astrophysics **651** (2021), A109
[14] J.G. Sorce *et al.*, arXiv preprint arXiv:2301.01305 (2023)
[15] C. Gouin *et al.*, Astronomy & Astrophysics **664** (2022), A198
[16] C. Gouin *et al.*, arXiv preprint arXiv:2306.04694 (2023)
[17] I. Vurm *et al.*, Astronomy & Astrophysics **673** (2023), A62
[18] M. Markevitch *et al.*, Physics Reports **443** (2007), 1
[19] A.J. Young *et al.*, The Astrophysical Journal **579** (2002), 560
[20] D.E. McLaughlin *et al.*, The Astronomical Journal **117** (1999), 2398
[21] I.D. Karachentsev *et al.*, Doklady Akademii Nauk Armânskoj SSR **42** (1966), 294
[22] G. De Vaucouleurs *et al.*, The Astrophysical Journal **202** (1975), 610
[23] D.I. Makarov *et al.*, Proceedings of the International Astronomical Union **11** (2014), 209

[1] https://localization.ias.universite-paris-saclay.fr